Electrical Contacts to One- and Two-Dimensional Nanomaterials

François Léonard[1]* and A. Alec Talin[2†]

Nanostructures such as carbon nanotubes, nanowires and graphene are being intensively explored for future electronic, photonic, and energy applications. In order for these nanosystems to progress from the research laboratory to technology, it is critical to precisely understand and control charge injection at the electrical contacts. While the scientific community and the semiconductor industry have invested significant resources to develop and control contacts to bulk semiconductor materials, charge injection at metal/nanostructure interfaces has received much less attention despite the obvious technological importance. Because nanostructures possess unique properties that differ significantly from bulk semiconductors, existing models of electrical contacts in bulk devices are often inapplicable at the nanoscale. In this review, we discuss experimental and theoretical work that has highlighted the much different physics and materials science of electrical contacts to nanostructures, and the key research and development challenges that must be addressed to understand and control nanocontacts.

The transport of electrical charge has become the working principle behind a breadth of modern day technologies. Indeed, electron flow governs the behavior of microelectronics components, the generation of solar power, the performance of photodetectors, the efficiency of energy storage, and provides lighting. The high performance of such technologies requires exquisite control over the charge carriers, which is intimately related to control over charge injection into the active material by electrical contacts. The importance of such contacts has been recognized early on in technology development, and has spurred tremendous efforts in learning to engineer such contacts to optimize device performance. This technology development has lead to a considerable body of work in basic science to understand the fundamentals of electrical contacts.

The constant drive towards improved technology has lead researchers to explore nanomaterials as replacements to conventional materials, due to their unique electronic, optical, thermal, and mechanical properties. Of these nanomaterials, carbon nanotubes, semiconductor nanowires, and graphene have attracted the greatest interest and scrutiny, and many laboratory demonstrations of nanodevices have been realized using these nanostructures (Fig. 1). A common element of these systems is the presence of metal/nanostructure interfaces for electron injection and extraction. As mentioned earlier, a high level of knowledge has been achieved for such electrical contacts to conventional, bulk materials, which is essential for high performance technology. However, given the

[1] Sandia National Laboratories, Livermore, California, 94551, USA. [2] Center for Nanoscale Science and Technology, National Institute of Standards and Technology, Gaithersburg, Maryland, 20899, USA. *email: fleonar@sandia.gov. †email: atalin@nist.gov

much different dimensionality and properties of nanostructures, electrical contacts to these materials are expected to behave much differently, and developing a fundamental understanding of their properties is essential for nanodevices to proceed from laboratory demonstrations into technology.

To explain the new challenges facing electrical contacts to carbon nanotubes, nanowires, and graphene, we begin by discussing the band alignment at metal/nanostructure interfaces. We then address charge injection phenomena before proceeding to a discussion of materials issues. A specific example of contacts to semiconductor nanowires is provided, and the review concludes with a discussion of the science and technology opportunities to develop high performance contacts to nanostructures.

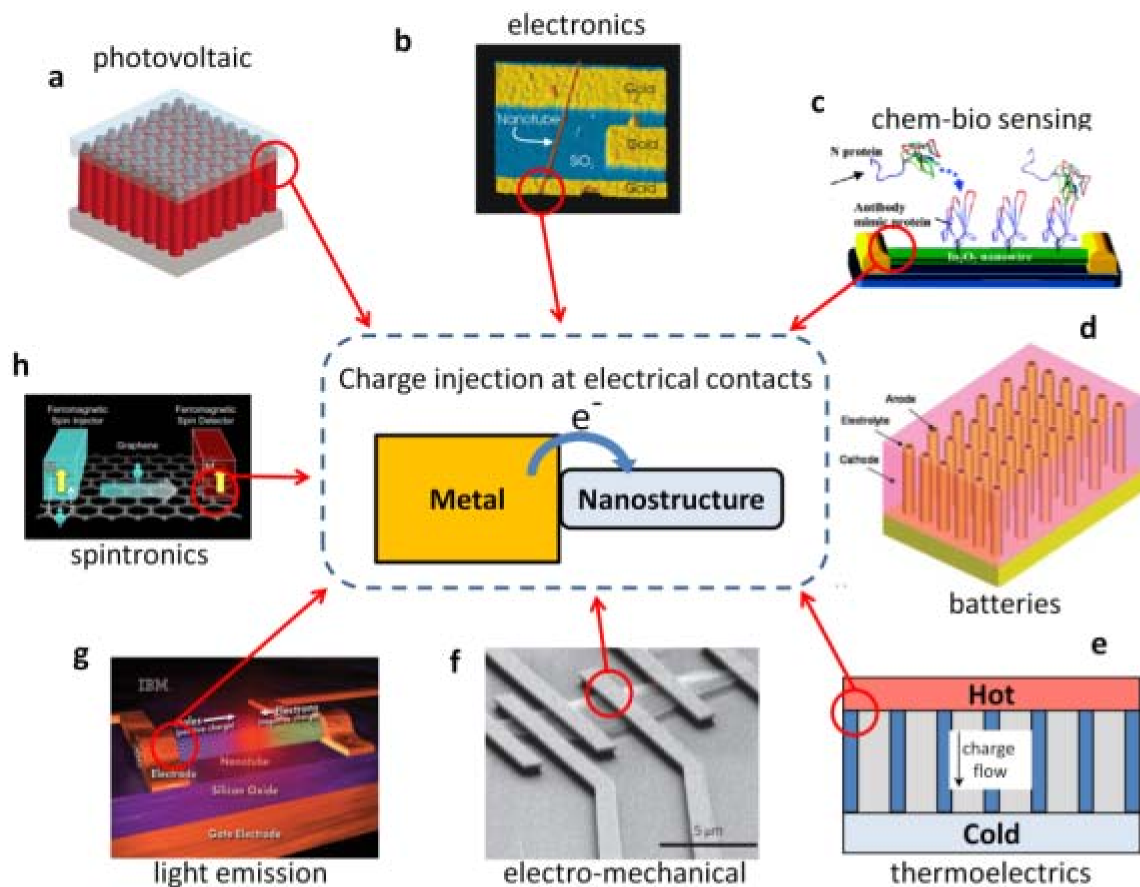

Figure 1 | Examples of nanomaterials-based devices. **a**, Photovoltaic device using an array of semiconducting nanowires. **b**, Carbon nanotube field-effect transistor. **c**, Chem-bio sensor with a functionalized semiconducting nanowire. **d**, Battery using an array of nanowires. **e**, Thermoelectric power generation or cooling with arrays of nanowires. **f**, Graphene nano electro-mechanical system. **g**, Light emission from a carbon nanotube device. **h**, Graphene-based spintronics. A commonality to all of these devices is the presence of a metal/nanostructure contact where charge injection occurs. Figures reproduced with permission from: **a**, Ref. 1; **b**, Ref 17**;** **c**, Ref. 2; **d**, Ref. 3; **f**, Ref. 4; **g**, Ref. 5; **h**, Kawawaki lab, UC Riverside.

Before moving to the main section of the manuscript, we first establish a central concept that is important when discussing contacts to nanostructures. In a conventional metal/semiconductor contact, there is a general geometry where the metal and semiconductor form a planar interface. For nanocontacts however, there are multiple possible geometries, each with its unique properties. These can be divided in two main classes: *end-bonded* contacts and *side contacts* (Fig. 2). In the case of end-bonded contacts, the nanostructure abruptly ends at the contact, and atomic bonds are formed with the metal. For side contacts, the nanostructure is embedded in the metal, and the bonding may be weak (i.e. van der Waals) or strong, depending on the system under consideration.

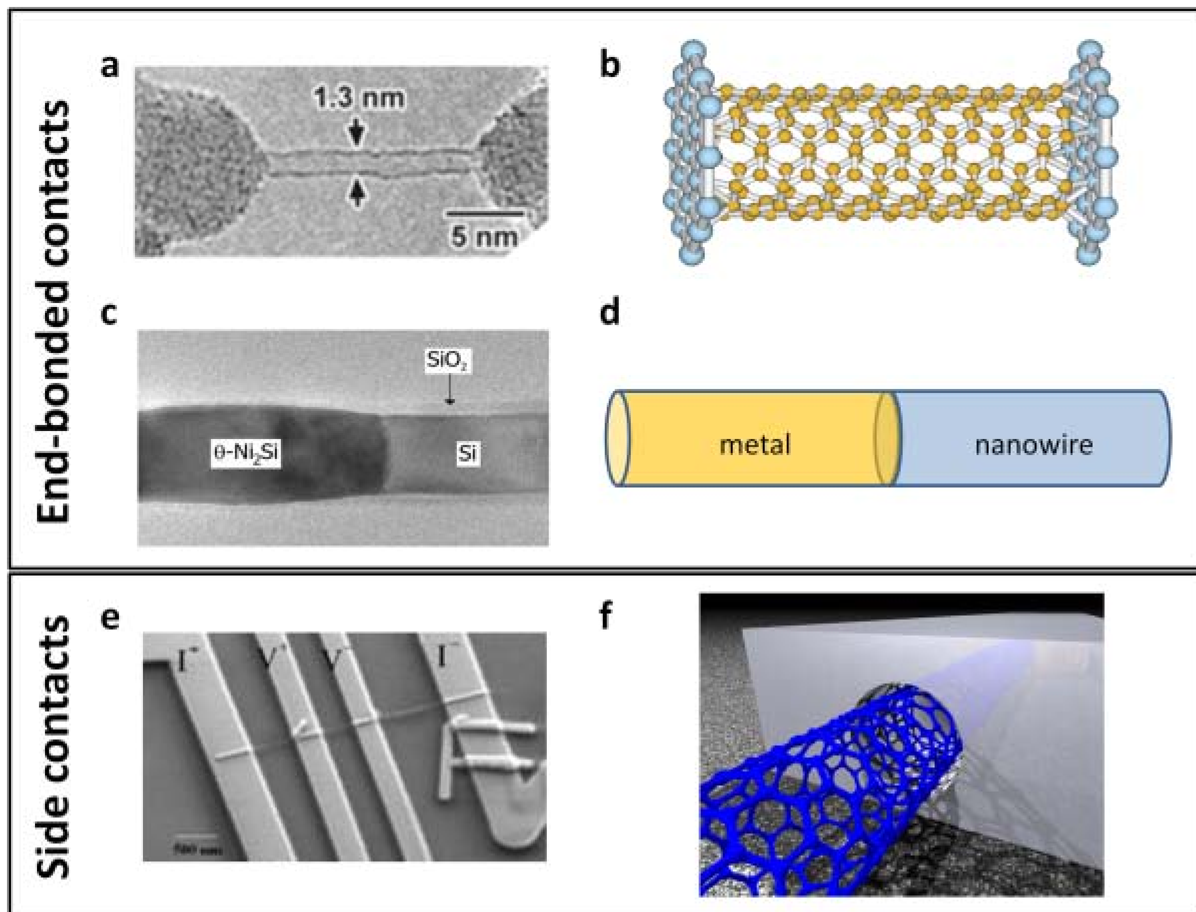

Figure 2 | Contact geometries. a-d, Two examples of end-bonded contacts to nanostructures. The top row shows a transmission electron micrograph of a carbon nanotube end-bonded to Ti contacts, with a schematic atomic representation. The bottom row shows a scanning electron micrograph of a Si nanowire end-bonded to NiSi with the associated schematic. **e,f**, Example of a side contact to a nanostructure. Scanning electron micrograph of several electrodes encapsulating a carbon nanotube, and illustration of the contact geometry. Figures reproduced with permission from: **a**, Ref. 6; **b**, Ref. 7; **c**, Ref. 8; **e**, Ref. 9.

Band alignment and band-bending

An important concept in understanding charge injection in nanostructures is the alignment of electronic energy levels directly at the metal/nanostructure interface. If the nanostructure is a semiconductor, then one is concerned with the alignment between the metal Fermi level and the conduction and valence bands of the semiconductor (Fig. 3a,b), while for a metallic nanostructure, the presence of a tunnel barrier is a key issue (Fig. 3c). In the case of Fig. 3a, the central interface property is the Schottky barrier ϕ_b, indicating that the metal Fermi level contacts the semiconductor in the bandgap. When the metal Fermi level is in the semiconductor conduction or valence band (Fig. 3b), the contact is called ohmic. This alignment of the metal Fermi level with the bandgap depends on many factors. The simplest model assumes that the Schottky barrier is determined by the difference between the metal workfunction and the semiconductor electron affinity: $\phi_b = \Phi - \chi$. However, because of the interaction between the semiconductor and the metal, electronic states appear in the semiconductor bandgap (Fig. 3d), and are often referred to as metal-induced gap states (MIGS). In bulk contacts, MIGS frequently determine completely the Schottky barrier, to such an extent that the metal workfunction often does not matter. However, in end-bonded[10] and side contacts to nanotubes and small nanowires[11], it has been suggested theoretically that MIGS have a much weaker impact on the band alignment due to electrostatics at reduced dimensions. Thus, one expects that the simple expression $\phi_b = \Phi - \chi$ will be a good description for some nanocontacts; this has been demonstrated experimentally in the case of contacts to carbon nanotubes[12,13]. The case of end-bonded contacts to nanowires[14] will be discussed in a later section.

In the absence of Fermi level pinning the band alignment for side contacts is determined by the charge transfer between the metal and the nanostructure, which occurs to equilibrate the Fermi level across the two materials. The charge transferred to the nanostructure is screened by the metal, or equivalently, an image charge appears in the metal; the resulting charge dipole leads to an electrostatic potential difference between the metal and nanostructure, which shifts the bands of the nanostructure. The final band alignment is thus determined by the transferred charge and the difference in electrostatic potential; a natural way to think about this is in terms of the capacitance between the metal and the nanostructure. As an example, the capacitance between a metal and a carbon nanotube is large because of the small dimensions; thus, the shift in potential is generally small, and the band alignment is determined mainly by the direct band-alignment between the metal Fermi level and the nanotube bandgap[11]. A similar situation arises for semiconducting nanowires, where the potential shift is accommodated in the nanowire, but because of the small cross-section, the appropriate band-bending cannot be established[11]. Graphene also displays charge transfer and re-alignment of the Fermi level when contacted by metals, an effect that also depends on the metal workfunction. Thus, contacts in graphene can be controlled from p-type to n-type simply by using metals of different workfunctions[15].

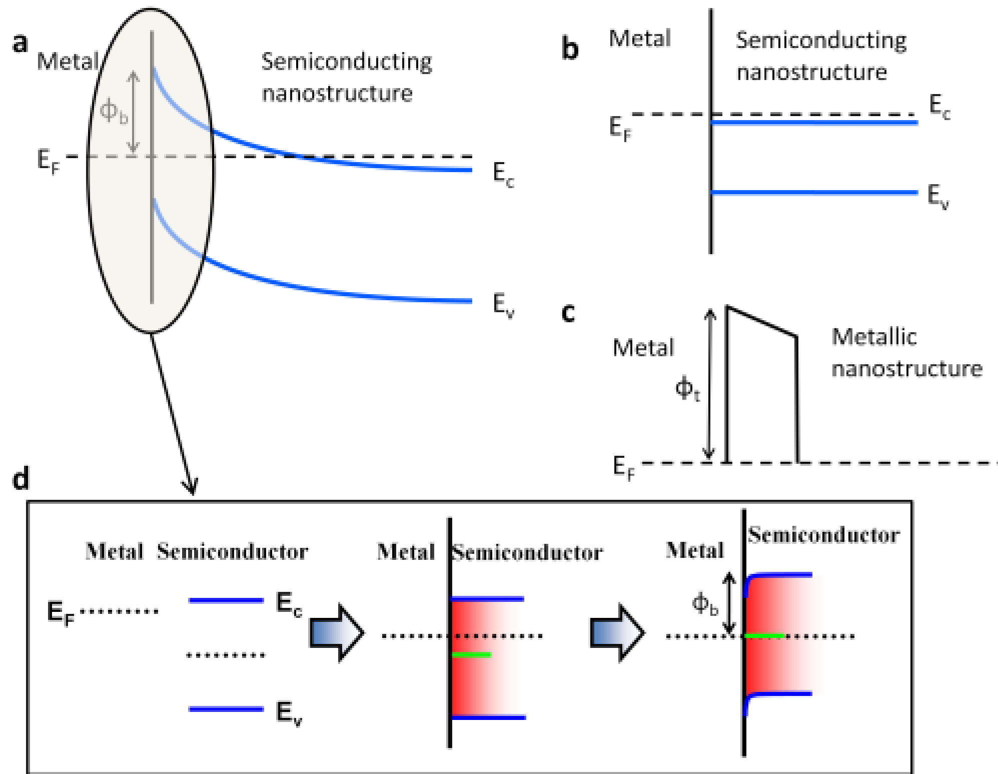

Figure 3 | Band alignment at metal/nanostructure interfaces. a, Band diagram for a Schottky contact, showing the conduction and valence band edges (E_c and E_v), the Fermi level (E_F), and the Schottky barrier (ϕ_b). **b**, Band alignment for n-type ohmic contact. **c**, For a metallic nanostructure, the presence of a tunnel barrier of height ϕ_t can govern the contact properties. **d**, In the near-interface region, the interaction with the metal causes electronic states to appear in the bandgap of the semiconductor; associated with these states is a charge neutrality level denoted by the green line. In general, the metal Fermi level will not be at the charge neutrality level, and a local band-bending will occur in the semiconductor to pin the Fermi level there.

Another important property of the metal/nanostructure interface is the band-bending away from the contact. While the band-bending due to Fermi level pinning is a near-interface phenomenon, the doping in the semiconductor also leads to band-bending, but on a length scale of tens of nanometers to microns. For bulk contacts, this length scale, called the depletion width, is given by $W=\sqrt{2\varepsilon\phi_b/ne}$ where ε is the dielectric constant, *n* is the dopant density, and *e* the electron charge. This expression is appropriate for nanostructures as long as it gives a length scale that is less than the nanostructure cross-section; otherwise, the nanostructure dimensions alter the electrostatics and lead to a size-dependent depletion width. In the case of carbon nanotubes, the cross-section is so small that only at very high doping is the bulk expression appropriate; in fact, at low and moderate doping levels, the depletion width is given instead by $W=R\exp\left(2\varepsilon_0\phi_b/\rho R\right)$ where *ρ* is the areal doping density and *R* is the nanotube radius[16]. Thus, *W* not only depends on the radius but is extremely sensitive to the doping level, and increases very rapidly at low doping. Experiments have confirmed the long distance band-

bending in nanotubes[17] and a similar phenomenon also arises in graphene, where the band-bending extends to hundreds of nanometers[18]. Modeling of end-bonded nanowires also demonstrated the diameter dependence of the depletion width[19]. As will be discussed in the next section, the size of the depletion width plays an important role in determining the charge injection processes that dominate the junction.

Charge injection

The band alignment concepts discussed in the previous section provide the basic equilibrium information necessary to understand charge injection at contacts. Understanding contacts then requires knowledge of the charge transport mechanisms that dominate the contact properties. In the presence of a Schottky barrier, the main transport mechanisms are thermionic emission over the Schottky barrier, tunneling through the barrier, and electron-hole recombination in the depletion region (Fig. 4). In thermionic emission, electrons in the metal absorb thermal energy from phonons, and are excited over the Schottky barrier, leading to an injection current that depends exponentially on voltage. In tunneling, electrons quantum mechanically tunnel through the barrier, causing a charge injection current that also depends exponentially on voltage, but is independent of temperature. The other mode of transport consists of electrons and holes simultaneously injected in the depletion region, which recombine directly or through defects, with the possible emission of a photon.

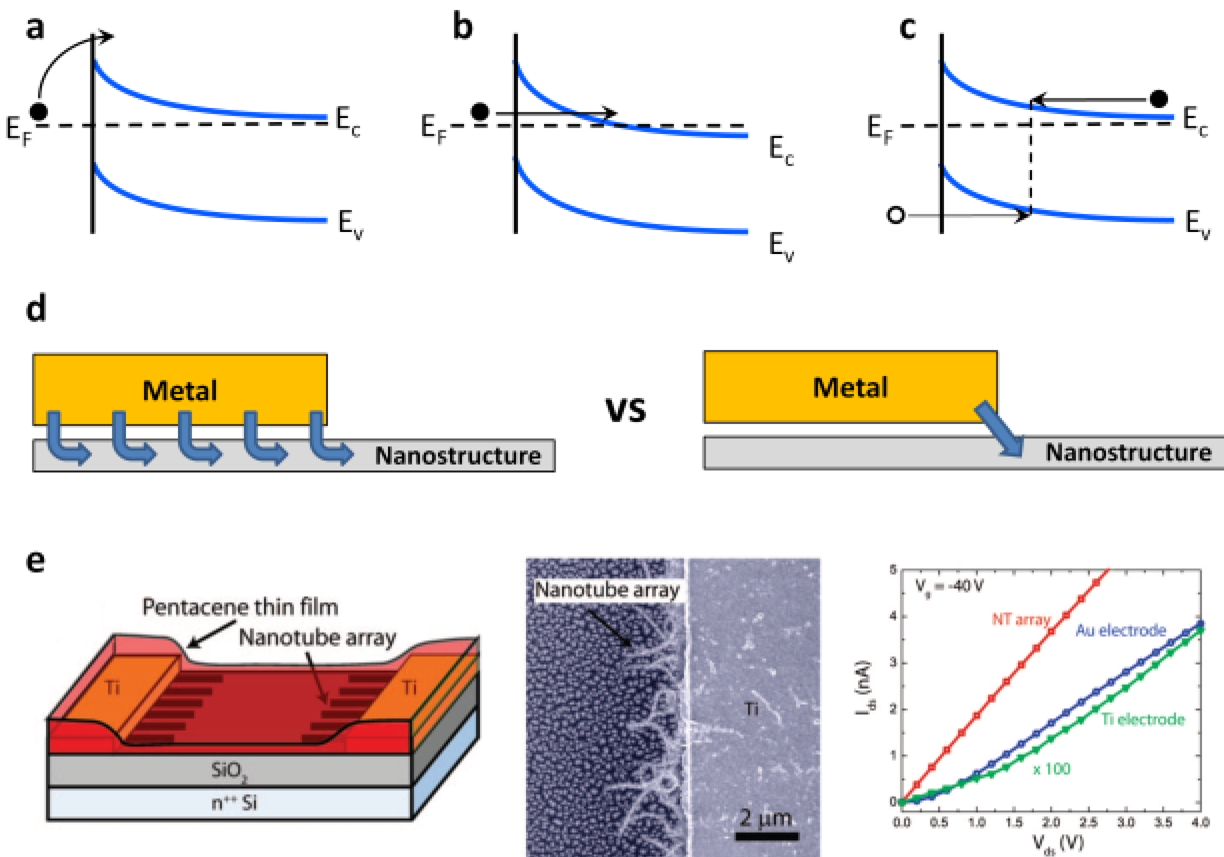

Figure 4 | Charge injection at metal/nanostructure contacts. a, Thermionic emission over a Schottky barrier. **b**, Tunneling through a Schottky barrier. **c**, Electron-hole recombination in the depletion region. **d**, Illustration of charge injection over the full length of the contact versus that at the edge of the contact. **e**, Charge injection from nanotube arrays into organic thin films. Figures reproduced with permission from: **e**, Ref. 20.

In the case of carbon nanotubes, the electrical characteristics of field-effect transistors made with moderate workfunction metals such as Ti have been shown to be dominated by Schottky barriers. For such devices, the charge injection (and device function) is determined by tunneling across the band-bending at the metal/nanotube contacts, which is controlled by the gate. Mixed modes of charge injection where tunneling and thermionic emission coexist are also possible, and have been observed in similar nanotube devices[21].

One approach to overcome Schottky barriers due to pinning at bulk metal/semiconductor junctions is to heavily dope the semiconductor near the contact in order to obtain a sharp band-bending, allowing for electrons to tunnel through the barrier. This approach is used extensively in modern semiconductor technology[22]. For end-bonded contacts to nanostructures, heavy doping can in principle work, because the necessary band-bending can be established along the length of the nanostructure. In the case of side contacts however, the situation is different, because the direction perpendicular to the metal/semiconductor interface is directly into the nanostructure cross-section. As a consequence, establishing the proper band-bending is difficult, and requires more and more doping as the nanostructure cross-section decreases in size[11]. This leads to reduced tunneling and a rapidly increasing contact resistance as the nanowire diameter is reduced.

Electron-hole recombination is not usually a mechanism that dominates transport at Schottky contacts. However, in some cases the height of the Schottky barrier is so large that both thermionic emission and tunneling are negligible; a prominent example is that of contacts to Ge nanowires[14]. The Ge-nanowire/metal interface is dominated by very strong Fermi level pinning that puts the Fermi level in the bandgap near the top of the valence band, regardless of the type of metal used. For n-type Ge, this leads to a large Schottky barrier for electrons of 0.59 eV, and little thermionic current. Charge injection is dominated by electron-hole recombination in the depletion region, but shows unusual properties compared to similar bulk injection: first, the recombination happens at the surface of the nanowire, leading to *increased* charge injection efficiency for smaller diameter nanowires. Second, the rapid increase of the depletion width with voltage at forward bias leads to a diameter-dependent ideality factor that deviates strongly from the bulk value. This case will be discussed in detail in a later section.

Another important aspect of charge injection that applies to side contacts has to do with the spatial location of the injection along the length of the contact (Fig. 4). The two limits correspond to injection along the whole length of the metal/nanostructure interface and injection at the edge of the contact. Theoretical work[23] has suggested that in the case of ballistic transport in metallic carbon nanotubes and graphene nanoribons, the coupling strength with the metal determines whether the injection is at the edge of the contact or along its length. Somewhat surprising is that strong coupling leads to edge injection, while weak coupling leads to length injection. This is explained from the large

perturbation that strong coupling imparts on the nanostructure at the edge of the contact, and the strong electron scattering that results, as opposed to weak coupling where the carriers can penetrate deeper in the contact. Recent experimental work on carbon nanotubes has studied this effect[24] and shown that the length of the metal contact on top of the nanotube directly determines the contact resistance, with smaller contact lengths giving higher resistance. In fact, the experimental data is well described by an inverse relationship between contact resistance and contact length, suggesting that charge injection takes place along the whole length of the metal/nanotube interface, at least for contacts less than 300 nm in length. This idea has recently been extended to palladium contacts to graphene, where it was suggested that the carrier mean-free path under the metal and the metal-graphene coupling length are intimately tied to determine the contact resistance[25].

We close this section by discussing how nanostructures can be used to improve the charge injection properties of the electrode itself. The idea is illustrated in Fig. 4e, where conventional electrodes are covered with carbon nanotubes that extend into the channel of a pentacene field-effect transistor. Because of their nanoscale dimensions, the electric field at the tips of the nanotubes is significantly enhanced compared to the planar metal-only electrode. This allows for very efficient charge injection in to the organic material; in fact, without optimization, the charge injection efficiency is three hundred times as large in this example compared with the planar metal electrode[20].

Materials issues

Realizing contacts with reproducible and stable electrical characteristics requires exquisite control over the structure and composition of the metal/semiconductor interface. Improved contact metallization for bulk Si, Ge, and compound semiconductor devices has been and continues to be the subject of intense research and development[22,26]. However, many of the schemes and processes developed for bulk devices have to be reevaluated when applied to nanostructures because of their very small volume, cross sectional area, and large surface-to-volume ratio. This is particularly important for integrating nanostructures into high performance electronics, where the source/drain series resistance becomes increasingly the limiting factor as other aspects of the device are optimized[27].

NiSi has become the preferred contact metallization in ultra large scale integrated Si circuits[28], and Ni-silicide reactions have recently been explored for contacting Si nanowires[29,30]. These studies have revealed that Ni reactions with Si nanowires proceed differently than those for bulk Si devices (Fig. 6). Specifically, the nanowire crystallographic orientation and the nanowire's ability to better accommodate strain can lead to stabilization of silicide phases not normally observed in bulk or thin film reactions under similar heat treatment. These distinct silicide phases can impact device performance because of higher sheet resistivity and higher Schottky barriers, and can potentially lead to catastrophic device failure if large built-in stress leads to extended defect formation. When a thin Ni film is deposited onto a Si substrate and annealed, the phase with the highest interdiffusion coefficient, the orthorhombic δ-Ni_2Si, forms first, followed by NiSi, and finally $NiSi_2$[28]. However, when Ni-silicide contacts are formed with [112] oriented Si nanowires, the hexagonal θ-Ni_2Si phase forms around 300 °C, even though in the bulk this phase is not observed until 800 °C. Despite having over 5 % difference in in-plane bond lengths along at least one direction perpendicular to the metal/nanowire interface, this phase

persists up to at least 600 ^{o}C; however, at 700 ^{o}C, the silicide forms outward growing whiskers (which could short neighboring devices) and a large number of twins due to the large compressive stress[29]. With (111) oriented Si nanowires (the most frequently observed growth direction) epitaxial $NiSi_2$ forms first and remains stable up to 700 ^{o}C, at which point the low resistivity NiSi forms; however the monosilicide is expected to revert back to $NiSi_2$ at slightly higher temperatures, thus potentially leaving a very narrow process window for the preferred phase formation, and the possibility of agglomeration during the higher temperature anneal.

Improved contact technology for Ge and group III-V compounds is currently an active area of research and development, spurred by the eventual need to replace Si with higher mobility semiconductors for high performance CMOS. However, few studies to date have focused on the contact metallurgy specific to nanowires made of these materials. Ni-germanides are similar in many respects to Ni-silicides and are currently being explored for contacting Ge nanowires[31]. The general strategy for making Ohmic contacts to III-V and II-VI nanowires, provided these have a sufficiently high carrier concentration ($>\approx 10^{18}/cm^3$) has been based on the use of Ti[32], or in some cases Al[33], both highly reactive metals with relatively low workfunctions, in combination with a low resistivity metal such as Au. Specific contact resistances, however, have not been thoroughly investigated.

As already pointed out, another significant materials challenge to realizing metal/nanostructure contacts with controlled electrical characteristics is the incorporation and activation of dopants. Bulk device doping techniques such as ion implantation or solid source in-diffusion lack the nanometer scale depth and spatial resolution necessary for uniformly doping nanowires, and in the case of ion implantation, also result in significant lattice damage. A recent approach that addresses this problem takes advantage of the self-limiting nature of some Si surface reactions to assemble uniform, dopant-containing molecular monolayers on the nanowire surface[34]. Once annealed, the dopants diffuse into the bulk of the nanowire, and a dopant concentration as high as $10^{19}/cm^3$ within a depth of 20 nm was demonstrated. The dopant concentration is controlled by the packing density of the dopant precursor: a relatively small P-containing molecule, 1-propylphosphonate, packs denser and leads to ≈10× higher doping than the larger trioctylphosphine oxide.

Reaction with the metal in the case of carbon nanotubes has been attempted by high temperature anneal of carbon nanotubes on Ti[6,35] to form TiC and end-bonded contacts, but these contacts possess a large Schottky barrier roughly equal to half of the nanotube bandgap. Recently, however it was reported that annealing carbon nanotubes contacted by Pt electrodes in vacuum above 900 K resulted in a sharp drop in contact resistivity[36]. These workers used X-ray photoemission spectroscopy, Raman spectroscopy, and electrochemical cyclic voltammetry to show that heating Pt in vacuum produced thin graphitic carbon layers on the surface, or graphene nanodomains, which they argue increase the electronic overlap between the metal and the carbon nanotube, effectively increasing the area of the contact. This result opens interesting avenues for studying nanomaterials for charge injection into other nanostructures[37,38].

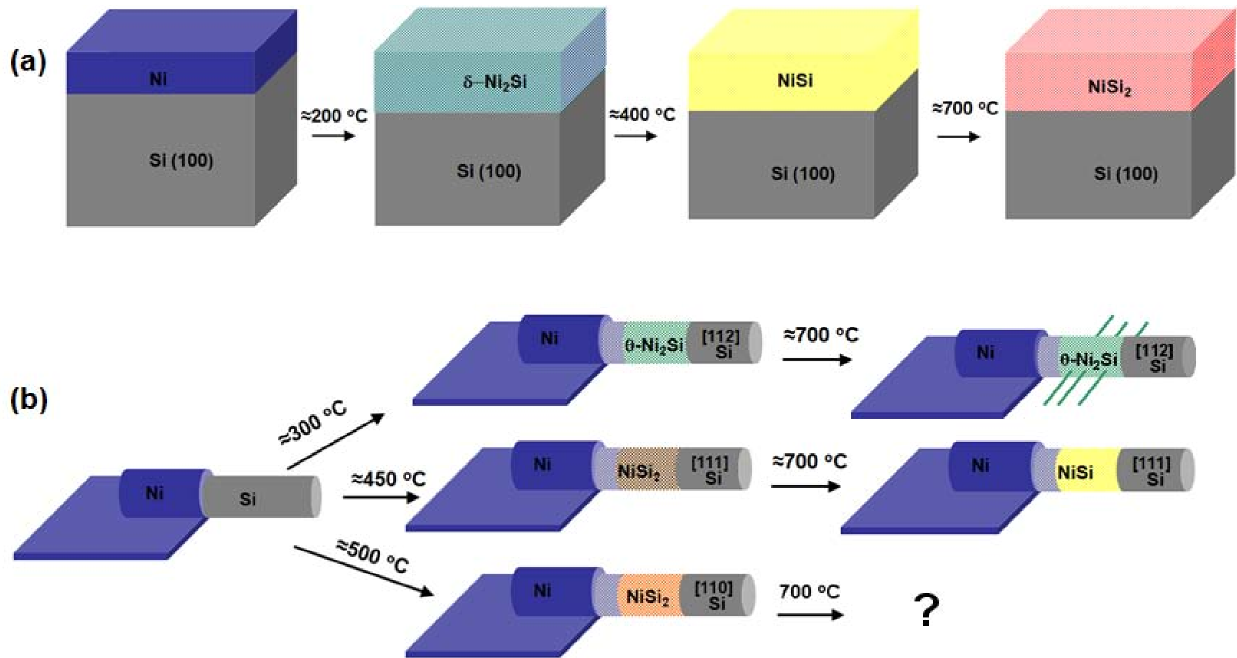

Figure 5 | Ni-Si phase formation sequence as a function of anneal temperature. a, Ni-silicides typically observed for a thin Ni film deposited on a (100) oriented Si wafer. **b**, Ni-silicides formed with Si nanowires strongly depend on nanowire crystallographic orientation. The presence of oxide on the nanowire surface and the starting amount of Ni can also affect the resulting silicide phase.

Case study: Au contacts to Ge nanowires

In this section, we use Au/Ge nanowire contacts to illustrate the practical aspects of the concepts discussed in the previous sections. Ge nanowire growth by chemical vapor deposition with Au catalyst nanoparticles on the substrate results in nanowire growth in the vapor-liquid-solid (VLS) mode. In this growth mode, a single-crystal Ge nanowire is formed, and the Au catalyst nanoparticle remains at the summit of the nanowire during and after growth (Fig. 6a, inset), providing a unique system to study nanocontacts. (A heavily doped Ge substrate serves at the other, Ohmic, contact). Atom-probe tomography measurements[39] and high-resolution transmission electron microscopy have indicated an abrupt interface between the Au-catalyst nanoparticle and the Ge nanowires[40]. Doping of the nanowires is accomplished during growth by using PH_3, leading to incorporation of P and n-type doping.

The inherent non-uniformity in Au nanoparticle dimensions leads to a variation in nanowire diameters which is ideal for investigating size effects on charge injection. Using a Au coated W STM tip retrofitted inside of a scanning electron microscope (see inset, Figure 6a) individual Au-Ge nanocontacts can be directly probed, giving rectifying current-voltage characteristics (Figure 6a). The rectifying current-voltage characteristics are consistent with that observed at bulk Au/Ge interfaces[41], where a large Schottky barrier of 0.59 eV is present, and is nearly independent of the type of metal due to strong Fermi level pinning close to the Ge valence band. Calculations show that this pinning of the Fermi level persists in the experimental nanowire geometry because of the high density of MIGS and the relatively large nanowire diameters.

Figure 6b shows I-V curves for four other nanowires plotted on a log-normal plot, revealing two surprising observations: (1) the current at small bias *increases* with decreasing diameter; and (2) the slope of the forward current versus bias *decreases* with decreasing diameter. These results imply strong size effects in nanocontacts. Figure 6c shows the small bias conductance for a large number of nanowires plotted versus diameter, clearly showing the rapid increase with decreasing nanowire diameter. This result is surprising, because it is generally believed that the increased importance of surface scattering should reduce the small-bias conductance density when the diameter is decreased. The observed phenomenon cannot be explained based on increased tunneling at smaller dimensions because the depletion width actually increases with decreasing diameter as we have seen in previous sections.

To understand these results, we consider the main carrier transport mechanisms characteristic of metal/semiconductor junctions that were introduced earlier: thermionic emission, tunneling, recombination in the space-charge region, and recombination in the neutral region[42]. As we already mentioned, tunneling can be discounted as the main transport mechanism in our case since the depletion width increases with decreasing diameter, thus lowering the tunneling probability. Thermionic emission, too, can be discounted, since the zero bias conductivity[42] $dJ/dV_{V=0} = \left(eA^{*}T^{2}/kT\right)\exp\left(-\phi_{b}/kT\right)$ where A^* is the Richardson's constant for Ge (50 Acm^{-2}K^{-2}), T is the temperature, k is the Boltzmann constant, and φ_b is the Schottky barrier (0.59 eV), predicts a current density of ≈0.01 A/cm^2, orders of magnitude lower than what is observed experimentally. Recombination in the neutral region also gives a zero bias conductivity that is at least two orders of magnitude too low. Thus, the only mechanism left is electron-hole recombination in the depletion region. This transport mechanism, which is frequently observed in situations with a relatively high Schottky barrier height and a low band gap[43] as is true for Au/Ge contacts, is characterized by the expression,

$$J_{rw} = J_{o}\left[\exp\left(\frac{eV}{nkT}\right) - 1\right] \qquad (1),$$

where J_o depends on the depletion width W and the minority recombination time τ according to $J_0 = eN_dW/\tau$, and n is the so-called ideality factor, equal to 2 for electron-hole recombination in the depletion region in bulk contacts. (As will be discussed below, $n = 2$ is consistent with the experimental observations in the large diameter limit.) The important point is that we expect an increase in W with decreasing diameter, and this is in qualitative accord with the results of Figure 6c.

To test this idea, we turn to numerical calculations of the electron-hole recombination current using the Shockley-Reed-Hall recombination model[42] . In this model, the small bias conductance can be evaluated from the expression

$$\left.\frac{dJ_{rd}}{dV}\right|_{V=0} = \frac{e}{kT}\frac{1}{\tau(d)}\int_0^L \frac{n_i^2}{n(z)+p(z)+2n_i}dz \qquad (2)$$

where *n(z)* and *p(z)* are the electron and hole concentrations as a function of distance z along the nanowire, and τ is written explicitly as a being a function of diameter. The key to evaluating the conductivity from this equation is finding the electron and hole concentrations as a function of z. This can be achieved by numerically simulating[14] the nanowire electrostatics in the geometry of Figure 6d. These calculations indicate that the depletion width *W* increases from approximately 30 nm for a nanowire of diameter of 90 nm, to almost 100 nm for a nanowire of 30 nm diameter. Thus, the increase in junction conductivity with decreasing diameter can be partially accounted for by the increase in the depletion width; indeed, the dashed line in Fig. 6c represents the zero bias conductivity calculated from Eq. (2) using the bulk recombination time. While this can explain some of the increase, to account for the much larger increase in zero bias conductivity observed experimentally, the dependence of the recombination time *τ* on the nanowire diameter has to be considered. Indeed, it is well known that unpassivated semiconductor surfaces represent excellent recombination sites. In nanowires, the surface-to-volume ratio increases as the diameter becomes smaller, thus leading to a dependence of the recombination time on the nanowire diameter. Formally, this problem can be solved by considering an infinitely long nanowire into which carriers are injected initially. These carriers relax by diffusing through the nanowire and recombining at the surface and in the bulk, leading to the following expression for the effective life time[14],

$$\frac{1}{\tau} = \frac{1}{\tau_{bulk}} + \frac{4s}{d} \qquad (3).$$

where s is the so-called surface recombination velocity typically used to analyze recombination at planar surfaces. With this diameter-dependent recombination time an excellent fit to the experimental data can be obtained (solid line in Figure 6c), and yields a recombination velocity of 2×10^5 cm/s, in agreement with a value recently measured by ultrafast pump-probe spectroscopy on nanowires prepared in the same growth chamber[44].

As mentioned earlier, the ideality factor for electron-hole recombination in the depletion region for bulk metal/semiconductor is $n=2$. This value is consistent with that extracted for nanowires of diameters larger than 80 nm (Figure 6c); however, at smaller diameters there is a strong increase of the ideality factor. This can be explained from the strong dependence of the depletion width on applied voltage compared to the usual case of bulk junctions, a consequence of the different electrostatics at reduced dimensions, as we have seen in previous sections. For bulk semiconductors, the depletion width depends on the square of the applied bias $W_{bulk} = \sqrt{2\varepsilon\varepsilon_o\left(V_{bi}-V\right)/N_d e}$, where V_{bi} is the built-in voltage and N_d is the dopant concentration. This mild dependence on voltage does not affect the exponential term in Equation (1). However, for nanowires one can derive that $W_{nw} \approx d\exp\left(8\varepsilon_o W_{bulk}^2/\varepsilon d^2\right)$, or $W_{nw} \propto \exp\left(-16\varepsilon_o V/eN_d\right)$. This strong voltage dependence

combines with the exponential term in Equation (1) leading to $J_{rw} \sim \exp\left(eV / n_{eff} kT\right)$, where $n_{eff} = 2 / \left(1 - l^2 / d^2\right)$ and $l = \sqrt{32kT\varepsilon_o / e^2 N_d}$. A fit of this last expression to the experimental data yields the screening length *l*=22 nm, which compares reasonably well with the value expected based on the estimated experimental carrier concentration. Thus, the electrostatics at reduced dimensions not only affects the low bias charge injection efficiency but also impacts the large voltage exponential increase of the current.

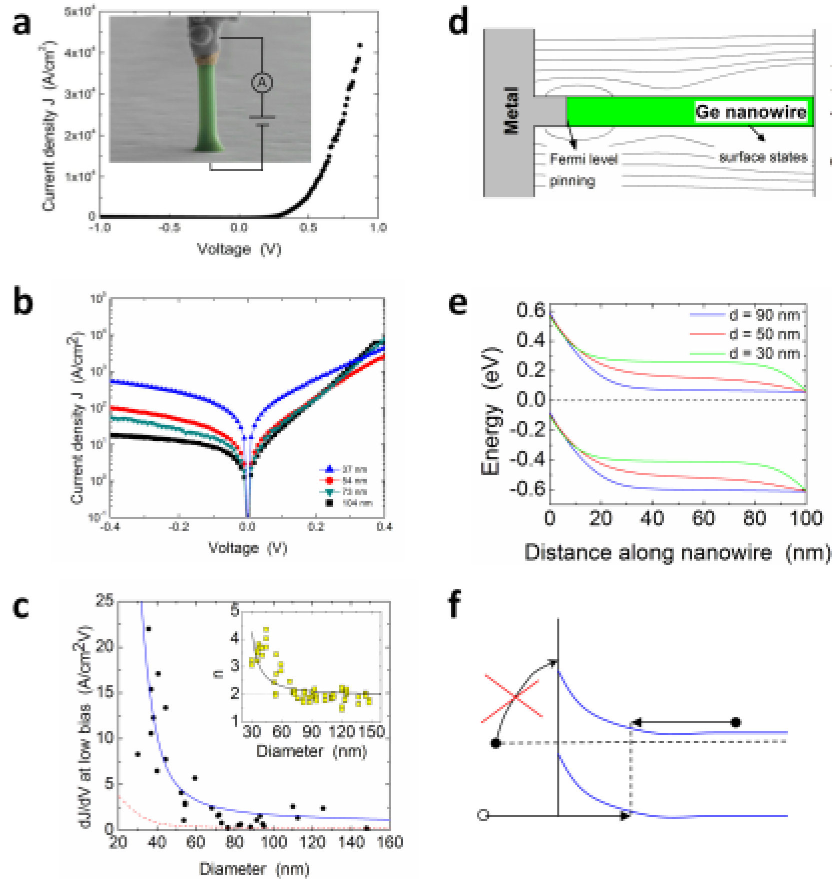

Figure 6 | Au-nanoparticle/Ge-nanowire contacts. a, Scanning electron microscope image of a Ge nanowire with a Au nanoparticle at its summit, contacted by a conducting probe, and the resulting I-V curve. **b**, Measured current-voltage characteristics for nanowires of different diameters. **c**, Low bias conductance and ideality factor as a function of diameter. **d**, Sketch of system used for numerical simulations. **e**, Calculated band-bending along the length of the nanowire. **f**, Charge injection is dominated by electron-hole recombination in the depletion region (Ref. 14).

Science and technology challenges and opportunities

To fully harness the properties of one- and two-dimensional nanomaterials, a better fundamental understanding of their properties is needed, as well as new approaches for technologically

realizing high performance contacts (Fig. 7). This requires new theoretical and experimental insights. For example, most existing concepts for the electronic properties of metal/nanostructure contacts assume that the electronic structure of the nanomaterials is unaffected, or only slightly disturbed by the presence of the metal. However, this may not necessarily be the case since the metal provides a new type of screening environment that could substantially impact the electronic properties. Indeed, the electron-electron interaction depends sensitively on the dielectric response of the system, and recently it was demonstrated through many-body ab initio approaches that the presence of acoustic plasmons in one-dimensional materials can significantly renormalize the bandgap[45]. Fundamental research is needed to develop and implement such many-body approaches in the context of contacts. To validate these computational approaches, it is necessary to experimentally measure the electronic and structural properties of the contacts. This is a challenging problem because of the small contact area for end-bonded contacts, and because the nanomaterial is embedded in the metal for side contacts. The later is a particularly acute problem, and only recently has progress been made in using scanning tunneling electron microscopy to image the structure of nanotubes embedded in a metal[46]; further work is needed to improve the spatial resolution and to obtain information on the electronic structure.

As we have seen in earlier sections, an important aspect of contacts is the control of doping in the semiconductor. For bulk contacts, procedures have been developed (e.g. ion implantation) and refined to precisely control contact properties. The understanding of dopant properties in nanostructures has not reached this level of understanding. For example, it is only recently that the dopants in nanowires have been imaged using atom probe tomography[47], revealing that their spatial distribution is nonuniform. Thus, understanding the role of nonuniform dopant distribution on contact properties is essential, as is understanding the origin of this distribution, and developing approaches to control it.

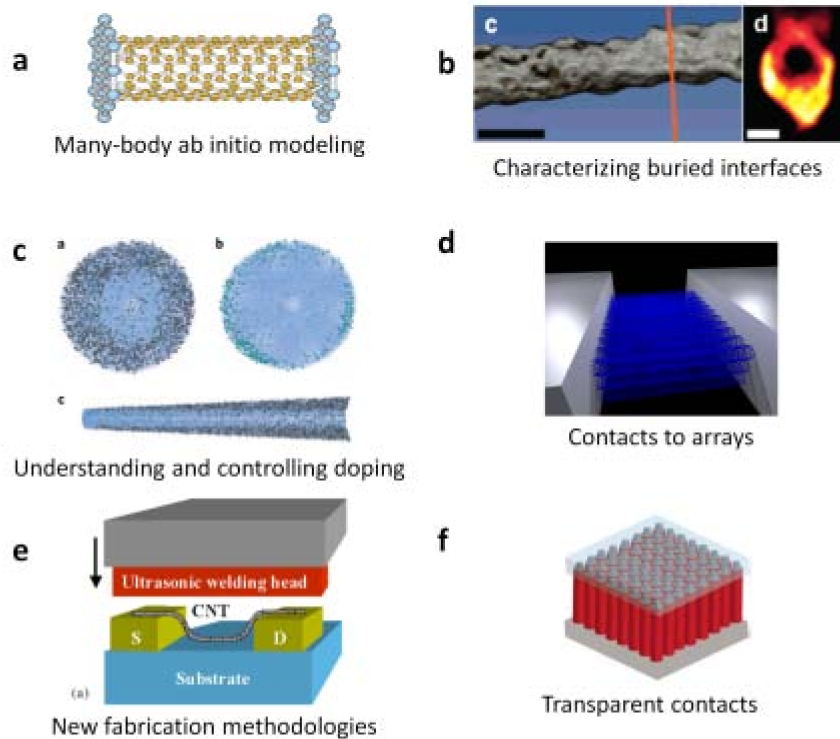

Figure 7 | Opportunities and challenges for research and development. a, Many-body ab initio modeling approaches. **b**, Experimental techniques to characterize the structural and electronic properties of buried interfaces. **c**, Experiments and theory to understand dopant distribution. **d**, Developing approaches to make contacts to arrays of nanostructures. **e**, New fabrication approaches to make contacts. **f**, Transparent contacts to nanostructures. Figures reproduced with permission from: **a**, Ref. 7, © YEAR Publisher; **b**, Ref. 46, © YEAR Publisher; **c**, Ref. 47, © YEAR Publisher; **e**, Ref. 1, © YEAR Publisher; Ref. 48, © YEAR Publisher.

A fundamental understanding of contact properties is not sufficient to bring nanodevices from laboratory demonstrations to technology. Indeed, for this to happen, technological approaches are needed that allow for rapid, repeatable, and reliable contact formation. While much discussion has focused on devices using individual nanostructures, many technological implementations will require arrays or thin films of nanostructures. The challenge there is that conventional deposition of metals on the array would only contact the top layer of the array/thin film, necessitating hopping between the individual nanostructures to transport the injected current. A better approach might be one where all of the nanostructures are directly contacted by the metal. Some approaches developed in the context of individual nanostructures may provide a path in this direction. For example, a new technique, termed "ultrasonic welding" has been developed whereby a welding head vibrating at ultrasonic frequencies is pressed on carbon nanotubes in contact with metals[48]. The vibration energy is sufficient to induce a reaction between the nanotube and the metal, essentially melting the two together. A related high temperature process has also been implemented for contacts to individual carbon nanotubes, whereby Ti is reacted with the nanotube to form TiC[6]; an intriguing question is whether this can be applied to arrays or thin films.

Transparent contacts are another important technology area, being critical for solar cell applications. While nanomaterials have been studied as replacement for existing transparent contact materials, a different question is how to make transparent contacts to the active area of a solar cell composed of nanomaterials. A specific example would be arrays of vertical nanowires, which require a top transparent contact; research and development work is needed to understand the structural properties of such contacts and the band alignment, as well as to develop fabrication approaches to realize high performance contacts. Work in this direction has already demonstrated that conventional transparent contact materials such as Indium Tin Oxide (ITO) can be utilized to realize nanowire array solar cells with reasonable energy conversion efficiencies[49].

Acknowledgements

F.L. acknowledges financial support from the Laboratory Directed Research and Development Program at Sandia National Laboratories, a multiprogram laboratory operated by Sandia Corporation, a Lockheed Martin Company, for the United States Department of Energy under contract DE-AC04-94-AL85000.

Additional information

The authors declare no competing financial interests.

References

1. Peters, C. H., Guichard, A. R., Hryciw, A. C., Brongersma, M. L. & McGehee, M. D. Energy transfer in nanowire solar cells with photon-harvesting shells. *J. Appl. Phys*. **105,** 124509 (2009).
2. Ishikawa, F. N. *et al*. Label-free, electrical detection of the SARS virus N-protein with nanowire biosensors utilizing antibody mimics as capture probes. *ACS Nano*. **5,** 1219-1224 (2009).
3. Dunn, B., Long, J. W., Rolison, D. R. Rethinking multifunction in three dimensions for miniaturizing electrical energy storage. *Electrochem. Soc. Interface* **17,** 49-53 (2008).
4. Chen, C. *et al.* Performance of monolayer graphene nanomechanical resonators with electrical readout. *Nature Nanotech*. **4,** 861-867 (2009).
5. Misewich, J. A., Martel, R., Avouris, Ph., Tsang, J. C., Heinze, S., Tersoff, J. Electrically induced optical emission from a carbon nanotube FET. *Science* **300,** 783-786 (2003).
6. Zhang, Y., Ichihashi, T., Landree, E., Nihey, F. & Iijima, S. Heterostructures of singlewalled carbon nanotubes and carbide nanorods. *Science* **285,** 1719-1722 (1999).
7. Palacios, J. J., Pérez-Jiménez, A. J., Louis, E., SanFabían, E. & Vergés, J. A. First principles phase-coherent transport in metallic nanotubes with realistic contacts. *Phys. Rev. Lett*. **90,** 106801 (2003).
8. Woodruff, S. M. *et al.* Nickel and nickel silicide Schottky barrier contacts to n-type silicon nanowires. *J. Vac. Sci. Technol*. B **26,** 1592-1596 (2008).
9. Zhang, Z., Dikin, D. K., Ruoff, R. S., Chandrasekhar, V. Conduction in carbon nanotubes through metastable resonant states. *Europhys. Lett*. **68,** 713-719 (2004).
10. Léonard, F. & Tersoff, J. Role of Fermi-level pinning in nanotube Schottky diodes. *Phys. Rev. Lett*. **84,** 4693-4696 (2000).
11. Léonard, F & Talin, A. A. Size-dependent effects on electrical contacts to nanotubes and nanowires. *Phys. Rev. Lett*. **97,** 026804 (2006).

12. Chen, Z., Appenzeller, J., Knoch, J., Lin, Y.-M., & Avouris, Ph. The role of metal-nanotube contact in the performance of carbon nanotube field-effect transistors. *Nano Lett*. **5,** 1497-1502 (2005).
13. Kim, W. *et al.* Electrical contacts to carbon nanotubes down to 1 nm in diameter. *Appl. Phys. Lett.* **87,** 173101 (2005).
14. Léonard, F., Talin, A. A., Swartzentruber, B. S., Picraux, S. T. Diameter-dependent electronic transport properties of Au-catalyst/Ge-nanowire Schottky diodes. *Phys. Rev. Lett.* **102,** 106805 (2009).
15. Giovannetti, G., Khomyakov, P. A., Brocks, G., Karpan, V. M., van den Brink, J., & Kelly, P. J. Doping graphene with metal contacts. *Phys. Rev. Lett.* **101,** 026803 (2008).
16. Léonard, F. *The Physics of Carbon Nanotube Devices* (William-Andrew, 2008).
17. Bachtold, A., Hadley, P., Nakanishi, T. & Dekker, C. Logic circuits with carbon nanotube transistors. *Science* **294,** 1317-1320 (2001).
18. Mueller, T., *et al.* Role of contacts in graphene transistors : a scanning photocurrent study. *Phys. Rev. B* **79,** 245430 (2009).
19. Hun, J., Liu, Y., Ning, C. Z., Dutton, R., & Kang, S.-M. Fringing field effects on electrical resistivity of semiconductor nanowire-metal contacts. *Appl. Phys. Lett.* **92,** 083503 (2008).
20. Aguirre, C. M., Ternon, C., Paillet, M., Desjardins, P., Martel, R. Carbon nanotubes as injection electrodes for organic thin film transistors. *Nano Lett.* **9,** 1457-1461 (2009).
21. Appenzeller, J., Radosavljevic, M., Knoch, J. & Avouris, Ph. Tunneling versus thermionic emission in one-dimensional semiconductors. *Phys. Rev. Lett.* **92,** 048301 (2004).
22. Brillson, L. J. *Contacts to Semiconductors: Fundamentals and Technology* (Noyes, 1993).
23. Nemec, N., Tománek, D., & Cuniberti, G. Contact dependence of carrier injection in carbon nanotubes : an ab initio study. *Phys. Rev. Lett*. **96,** 076802 (2006).
24. Franklin, A. D. & Chen, Z. Length scaling of carbon nanotube transistors. *Nature Nanotech*. **5,** 858-862 (2010).
25. Xia, F., Pereibenos, V., Lin, Y.-M., Wu, Y., & Avouris, Ph. The origins and limits of metal-graphene junction resistance. *Nature Nanotech*. **6,** 179-184 (2011).
26. Dimoulas, A. *et al.* Source and drain contacts for germanium and III-V FETs for digital logic. *MRS Bull*. **34,** 522-529 (2009).
27. King, T.-J. Taking silicon to the limit. *Electrochem. Soc. Interface* **14,** 38-42 (2005).
28. Lavoie, C. *et al.* Towards implementation of a nickel silicide process for CMOS technologies. *Microelec. Eng.* **70,** 144-157 (2003).
29. Dellas, N. S. *et al.* Orientation dependence of nickel silicide formation in contacts to silicon nanowires. *J. Appl. Phys.* **105,** 094309 (2009).
30. Lin, Y.-C. *et al.* Growth of nickel silicides in Si and Si/SiOx core/shell nanowires. *Nano Lett*. **10,** 4721-4726 (2010).
31. Dellas, N. S. *et al.* Formation of nickel germanide contacts to Ge nanowires. *Appl. Phys. Lett*. **97,** 263116 (2010).
32. Talin, A. A. *et al.* Correlation of growth temperature, photoluminescence, and resistivity in GaN nanowires. *Appl. Phys. Lett*. **92,** 093105 (2008).
33. Lee, T. I. *et al.* Electrical contact tunable direct printing route for a ZnO nanowire Schottky diode. *Nano Lett.* **10,** 3517-3523 (2010).
34. Ho, J. C. et al. Controlled nanoscale doping of semiconductors via molecular monolayers. *Nature Mater.* **7,** 62-67 (2008).
35. Martel, R. *et al*. Ambipolar electrical transport in semiconducting single-wall carbon nanotubes. *Phys. Rev. Lett*. **87,** 256805 (2001).
36. Kane, A. A. *et al*. Graphitic electrical contacts to metallic single-walled carbon nanotubes using Pt electrodes. *Nano Lett*. **9,** 3586-3591 (2009).

37. Jang, S. *et al*. Flexible, transparent single-walled carbon nanotube transistors with graphene electrodes. *Nanotechnology* **21,** 425201 (2010).
38. Li, B. *et al*. All-Carbon electronic devices fabricated by directly grown single-walled carbon nanotubes on reduced graphene oxide electrodes. *Adv. Mater*. **22,** 3058–3061 (2010).
39. Perea, D. E., Wijayaa, E., Lensch-Falk, J. L., Hemesath, E. R., & Lauhon, L. J. Tomographic analysis of dilute impurities in semiconductor nanostructures. *J. Solid State Chem*. **181,** 1642-1649 (2008).
40. Taraci, J. L., Dailey, J. W., Clement, T., Smith, D. J., Drucker, J. & Picraux, S.T. Nanopillar growth mode by vapor-liquid-solid epitaxy. *Appl. Phys. Lett*. **84,** 5302-5304 (2004).
41. Nishimura, T., Kita, K., & Toriumi, A. Evidence for strong Fermi level pinning due to gap states at metal/germanium interface. *Appl. Phys. Lett*. **91,** 123123 (2007).
42. Sze, M. & Ng, K.K. *Physics of Semiconductor Devices*, *Third Edition* (Wiley 2007).
43. Rhoderick, E.H. & Williams, R.H. *Metal–Semiconductor Contacts*, Second Edition (Oxford Science Publications 1988).
44. Prasankumar, R. P. *et al*. Ultrafast electron and hole dynamics in germanium nanowires. *Nano Lett*. **8,** 1619-1624 (2008).
45. Spataru, C. D. & Léonard, F. Tunable bandgaps and excitons in doped carbon nanotubes made possible by acoustic plasmons. *Phys. Rev. Lett*. **104,** 177402 (2010).
46. Cha, J. J. *et al.* Three dimensional imaging of carbon nanotubes deformed by metal islands. *Nano Lett.* **7,** 3770-3773 (2007).
47. Allen, J. E., Perea, D. E., Hemesath, E. R., Lauhon, L. J. Nonuniforn nanowire doping profiles revealed by quantitative scanning photocurrent microscopy. *Adv. Mater.* **21,** 3067-3072 (2009).
48. Chen, C., Yan, L., Kong, E. S.-W., Zhang, Y. Ultrasonic nanowelding of carbon nanotubes to metal electrodes. *Nanotechnology* **17,** 2192-2197 (2006).
49. Czaban, J. A., Thompson, D. A. & LaPierre, R. R. GaAs core-shell nanowires for photovoltaic applications. *Nano Lett.* **9,** 148-154 (2009).